Modeling and experimental validation of TCE abatement and ozone formation with non thermal plasma

A. M. Vandenbroucke[1], R. Aerts[2], R. Morent[1], N. De Geyter[1], A. Bogaerts[2], C. Leys[1]
[1]Department of Applied Physics, Ghent University, Belgium
[2]Department of Chemistry, University of Antwerp, Belgium

Abstract—In this study, the formation of ozone and the abatement of trichloroethylene (TCE) with non thermal plasma was experimentally and theoretically investigated. The model predicts that the ozone formation increases with the energy deposition and decreases with the relative humidity (RH) of the air, which is qualitatively in agreement with experimental data. For an energy deposition of 0.136 J/cm³, the abatement of 1000 ppm TCE in air with 5 % RH is dominated by atomic oxygen and to a lesser extent by OH radicals. In the afterglow of the discharge, the destruction is dominated by the ClO radicals. An increase in RH reduces the reaction rates of TCE with atomic oxygen and ClO radicals but favors the destruction by OH radicals.

Keywords—Non thermal plasma, ozone formation, TCE, modeling

I. INTRODUCTION

Non-thermal plasma's (NTP) have been widely applied for the removal of volatile organic compounds (VOCs) from waste gas streams [1]. During the last two decades, much progress has been made in terms of reactor design and optimizing operating conditions to increase the effectiveness of the removal process. However, due to the creation of multiple reactive species in the active plasma zone, there is still a lack of insight in the underlying mechanisms that enable the removal of VOCs. Therefore, we have experimentally and theoretically investigated the abatement of dilute trichloroethylene (TCE) and the formation of ozone in air with NTP. The plasma-chemical model and experimental validation allow us to obtain a better understanding of the chemical processes occurring in the discharge. Moreover, it is possible to derive the degradation pathway of TCE, based on the distribution of intermediates and final byproducts. To our knowledge, only Evans *et al.* have performed such a study to investigate the removal of TCE from $Ar/O_2/H_2O$ mixtures with dielectric barrier discharges [2]. Recently, we have experimentally found that the decomposition of TCE has led to the formation of various by-products, including phosgene, dichloroacetylchloride, trichloroacetaldehyde, HCl, Cl_2, CO, CO_2 and O_3 [3].

For practical applications, the humidity of the air is an important parameter that affects the removal process significantly [1]. Therefore, the water content of the influent was varied and the outcome on the removal process was studied theoretically.

II. EXPERIMENTAL SET-UP

Corresponding author: A. M. Vandenbroucke
e-mail address: ArneM.Vandenbroucke@UGent.be

A. *Description of the model*

The simulations in this work are performed using the numerical model Global_kin developed by Dorai and Kushner [4]. In this model, two basic modules are used: the Boltzmann equation module and a zero-dimensional plasma chemistry module. First, a reaction mechanism is defined (see below). Next, the Boltzmann equation module uses the collision cross sections to calculate the values of the reaction rate coefficients of electron impact reactions, depending on the electron energy, and look-up tables containing this information will be created. These coefficients will then be used in the chemistry module to calculate the source terms for the gas phase reactions of the different species:

$$\frac{dn_i}{dt} = \sum_j [(a_{ij}^R - a_{ij}^L) k_j \prod_l n_l^L] \quad (1)$$

Where n_i is the density of species i, a_{ij}^R and a_{ij}^L are the right-hand side and left-hand side stoichiometric coefficients of species i in reaction j, k_j is the reaction rate coefficient of reaction j and n_l^L is the density of the l^{th} species in the left-hand side of reaction j. Note that no transport is included in this chemistry module. Indeed, the plasma reactor is considered as a batch reactor with a uniform concentration of species over the entire reactor volume.

The electron induced reactions depend on electron temperature, which changes, on one hand, due to Joule heating from the applied power, and on the other hand, due to the energy lost in collisions. The electron temperature is calculated from:

$$\frac{d}{dt}\left(\frac{3}{2} n_e k_B T_e\right) = \vec{j} \cdot \vec{E} - \sum_i \frac{3}{2} n_e \nu_{mi} \left(\frac{2m_e}{M_i}\right) k_B (T_e - T_i) + \sum_l n_e k_l N_l \Delta\varepsilon_l \quad (2)$$

where n_e is the electron density, k_B is Boltzmann's constant, T_e is the electron temperature, $\vec{j}$ and $\vec{E}$ are the current density and the electric field in the discharge respectively, ν_{mi} is the electron momentum transfer collision frequency with species i, m_e is the electron mass and, M_i and T_i are the mass and temperature respectively of species i. k_l is the reaction rate coefficient for the l^{th} electron impact process, N_i is the density of the gas phase collision partner and $\Delta\varepsilon_l$ is the corresponding change in the electron energy. Since the model is zero-dimensional, the product of current density with electric field is not used here, but instead, the ratio of the applied power to the plasma volume is used, which is equivalent.

The chemistry module is called every time step and the Boltzmann module is only called when the background gas density has significantly changed. Indeed, it is not necessary to call this Boltzmann module every time step. More details on the model can be found in the papers by Dorai and Kushner [4].

In this work, the Global_kin model was extended with a reaction analysis module in order to have an automatically printed overview of all the absolute contributions of the relevant reactions to the production and loss of all species. For the absolute contributions, (1) is used. Next to the absolute contributions, also the relative contributions of the relevant reactions to the production and loss of a species are calculated from:

$$\gamma_{ij} = \left(\left(a_{ij}^{R} - a_{ij}^{L} \right) k_j \prod_l n_l^{L} \right) / \left(\frac{dn_i}{dt} \right)_{prod/loss} \qquad (3)$$

where γ_{ij} is the relative contribution of reaction j to the production or loss of species i, which is always evaluated versus the total dn_{ij}/dt production or loss. All the other parameters have the same meaning as in (1).

B. Description of the chemistry

The chemistry used in the model contains 114 species and 1155 reactions. This high number of reactions is needed if a description of a complex medium like air is required. We have taken into account ions, electrons and neutrals as well as nitrogen and oxygen excited states. The complete reaction set can be obtained from the authors upon request

In literature, the destruction of TCE with NTP is described by many possible pathways [5]. The first pathway could be the electron attachment of TCE where TCE decomposes in C_2HCl_2 and a chlorine anion:

$$C_2HCl_3 + e^- \rightarrow C_2HCl_2 + Cl^- \qquad 3.0\times10^{-13}\ cm^3/s \qquad (4)$$

However the electron density of the corona discharge used for the application is quite small in comparison with other low temperature plasmas such as dielectric barrier discharges. As also the reaction rate coefficient of this process is indicated by a low value, the contribution of this reaction should be limited.

Another possible mechanism is the dissociation of TCE by reaction with atomic oxygen to numerous end products:

$$C_2HCl_3 + O \rightarrow CO + CCl_2 + HCl \qquad 2.3\times10^{-13}\ cm^3/s \qquad (5)$$
$$C_2HCl_3 + O \rightarrow CHOCl + CCl_2 \qquad 5.7\times10^{-13}\ cm^3/s \qquad (6)$$
$$C_2HCl_3 + O \rightarrow COCl + CHCl_2 \qquad 8.7\times10^{-14}\ cm^3/s \qquad (7)$$
$$C_2HCl_3 + O \rightarrow C_2Cl_3 + OH \qquad 6.3\times10^{-15}\ cm^3/s \qquad (8)$$

The rate coefficients are in the same order of magnitude as for the electron attachment process. Atomic oxygen has however a longer lifetime than the electrons and the reaction with atomic oxygen is therefore more likely to take place.

Especially in humid air, the dissociation of TCE can also be caused by reaction with hydroxyl radicals:

$$C_2HCl_3 + OH \rightarrow CHCl_2 + CHOCl \qquad 3.1\times10^{-13}\ cm^3/s \qquad (9)$$
$$C_2HCl_3 + OH \rightarrow C_2Cl_3 + H_2O \qquad 1.9\times10^{-12}\ cm^3/s \qquad (10)$$
$$C_2HCl_3 + OH \rightarrow C_2HCl_2OH + Cl \qquad 2.4\times10^{-13}\ cm^3/s \qquad (11)$$
$$C_2HCl_3 + OH \rightarrow CHCl_2COCl + H \qquad 2.4\times10^{-14}\ cm^3/s \qquad (12)$$

These rate coefficients also are in the same order of magnitude as the previously mentioned pathways, which suggests that again the densities of the reactants have a major influence on the actual rates of the different dissociation reactions.

There is also a possibility that TCE is decomposed by radicals originally produced by TCE as for example reactions with Cl or ClO radicals:

$$C_2HCl_3 + ClO \rightarrow CHCl_2 + COCl_2 \qquad 3.1\times10^{-12}\ cm^3/s \qquad (13)$$
$$C_2HCl_3 + Cl \rightarrow C_2Cl_3 + HCl \qquad 3.3\times10^{-12}\ cm^3/s \qquad (14)$$

These reactions have a rate coefficient one order higher than the previously mentioned reactions. However, these reactions can only be a secondary destruction process. Indeed, the densities of Cl and ClO are very low in the beginning but can increase very fast as Cl is a common dissociation product.

The final dissociation pathway considered in the model is the dissociation by metastable nitrogen species. Indeed those species were already indicated by *Blin-Simiand et al.* as dominant dissociation species for volatile organic compounds [6]. It is also indicated that the dissociation of TCE reaches a higher efficiency in nitrogen compared to air which suggests that metastable nitrogen species might play an important role in the dissociation of TCE [7]. As far as we know, no data of reaction rate coefficients for TCE with nitrogen metastables are published. Therefore, we assumed the following reactions in the model:

$$C_2HCl_3 + N_2(A^3\textstyle\sum_u^+) \rightarrow C_2HCl_2 + Cl + N_2 \qquad (15)$$

$$C_2HCl_3 + N_2(a') \rightarrow C_2HCl_2 + Cl + N_2 \quad (16)$$

The rate coefficients of these reactions were evaluated between 10^{-8} - 10^{-13} cm³/s, i.e., the typical range for reactions of nitrogen metastables with organic species, as found in literature [6].

C. Description of the experiments

The experimental set-up is shown in Fig. 1. A pressurized air bottle (Air Liquide, Alphagaz 1) delivers air to two mass flow controllers (Bronkhorst, El-Flow). Bubblers systems are used to set the TCE concentration and relative humidity (RH) of the gas stream. The initial TCE concentration and humidity are controlled by either adjusting the temperature of the water bath or by changing the flow rate of air through the bubbler system. Experiments are carried out with a total flow rate of 2 l min^{-1} which corresponds to a residence time of 1.47 s.

The multi-pin-to-plate plasma source is based on the concept of a negative DC glow discharge. The rectangular duct has a cross section of 40 mm × 9 mm and a length of 200 mm. The plasma source consists of five aligned cathode pins which were positioned 28 mm from each other. The distance between the five cathode pins and the single anode plate is 9 mm. The discharge is powered with a 30 kV/20 mA DC power supply and generated at atmospheric pressure and room temperature. A high voltage probe (Fluke 80 K-40, division ratio 1/1.000) measures the voltage applied to the electrode. The discharge current is determined by recording the voltage signal across a 100 Ω resistor placed in series between the counter electrode and ground. The threshold current for the glow-to-spark transition is increased by profiling the anode surface with hollow spherical surface segments centered on the tip of each crenellated cathode pin [8]. The spherical surface segment has a radius of curvature of 17.5 mm and a depth of 5 mm. Stable and uniform glow discharge operation is ensured by the fast gas flow and by ballasting each cathode pin with a 1.5 MΩ resistor.

FT-IR spectroscopy (Bruker, Vertex 70) is used to determine the in- and outlet concentration of TCE and to qualitatively analyze the formation of byproducts. The optical length of the adjustable gas cell and the resolution of the spectrometer are set at 0.80 m and 4 cm^{-1}, respectively. The formation of ozone is monitored with a UV-absorption (245 nm) analyzer (Advanced Pollution Instrumentation, API-M450) located downstream. The temperature and humidity are measured with a combined temperature/humidity sensor (Testo 445).

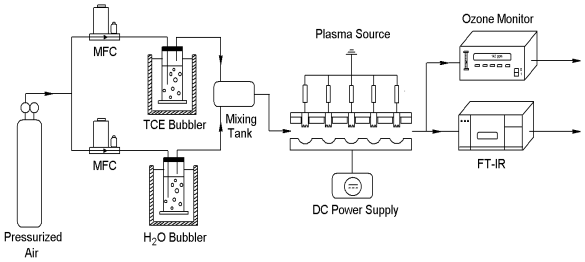

Fig. 1. Experimental set-up

III. Results

A. Ozone formation in pure air

As the model used in this work is a zero-dimensional model, the corona discharge can only be simulated as one power pulse or by a series of power pulses. At this moment, we are still evaluating those two power deposition cases and therefore we present here only results for the one pulse simulations. The amplitude (267 W) and the length (0.5 ms) of the pulse were artificially chosen to fit the values of the electron density (10^8 –10^9 cm^{-3}) and electron temperature (2-3 eV) expected in a typical pin-to-plate corona discharge [8].

To investigate the formation of ozone in the corona plasma, multiple simulations were performed for different energy depositions. Fig. 2 presents the density of ozone as a function of time for different values of energy deposition. It can be seen that the density of ozone increases with increasing energy deposition, which is also indicated by the experimental values illustrated in Fig. 3. Indeed, the experimental ozone concentrations increase linearly ($0.9935<R^2<0.9985$) with the energy density for each value of the relative humidity.

As the humidity of air is not a constant value, it is important to investigate the influence of humidity on the ozone formation. Fig. 4 shows the normalized ozone density as a function of time for different levels of humidity at an energy deposition of 0.136 J/cm³. Normalization is required to compare the results on one graph as they have a different background gas composition. The figure indicates that the ozone density decreases with increasing humidity, which is also indicated by the experimental values plotted in Fig. 3.

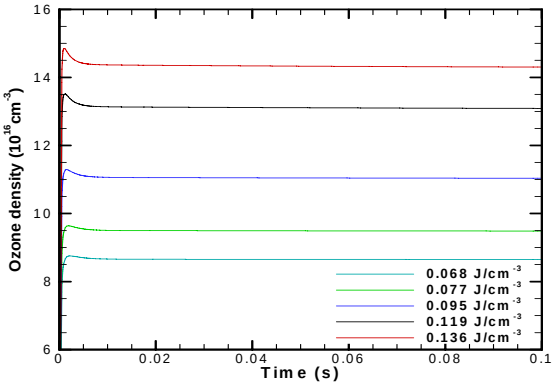

Fig. 2 Calculated ozone density as a function of time for different values of energy deposition in humid air (5% relative humidity).

Our calculations further predict that the production and loss of ozone is mainly dominated by the following reactions:

$$O + O_2 + M \rightarrow O_3 + M \qquad 6.0\times10^{-34}\ cm^6/s \quad (17)$$
$$NO + O_3 \rightarrow NO_2 + O_2 \qquad 4.3\times10^{-12}\ cm^3/s \quad (18)$$
$$O + O_3 \rightarrow O_2 + O_2 \qquad 8.0\times10^{-15}\ cm^3/s \quad (19)$$
$$e^- + O_3 \rightarrow O_2 + O + e^- \qquad 1.9\times10^{-9}\ cm^3/s \quad (20)$$

In general, the production of ozone is mainly dependent of the atomic oxygen production which is mainly produced by the electron impact dissociation of oxygen:

$$e^- + O_2 \rightarrow O + O + e^- \qquad 8.6\times10^{-10}\ cm^3/s \qquad (21)$$

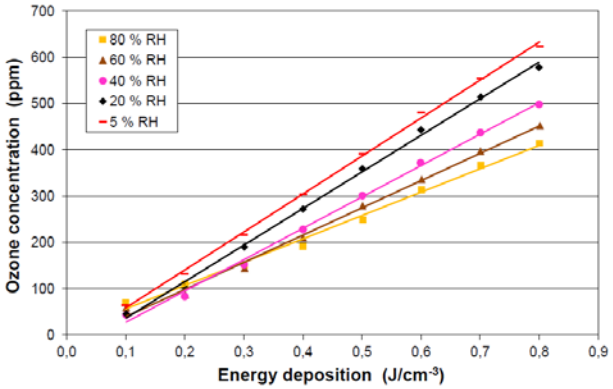

Fig. 3 Measured ozone concentration as a function of energy deposition for different values of relative humidity.

Indeed, this dissociation is dependent of the electron density and therefore also related to the power deposition in the plasma. This suggests that ozone is indirectly related to the electron density with an increasing density of ozone for an increasing electron density, as indicated in Fig. 2. If humid air is considered, the following reaction should also be taken into account as an ozone loss process:

$$OH + O_3 \rightarrow HO_2 + O_2 \qquad 7.3\times10^{-14}\ cm^3/s \qquad (22)$$

By increasing the humidity, the water density in the plasma increases, which favors the electron impact dissociation of water, therefore increasing the hydroxyl radical density:

$$e^- + H_2O \rightarrow OH + H + e^- \qquad 5.8\times10^{-10}\ cm^3/s \qquad (23)$$

Eventually the hydroxyl radicals react with ozone by (22) to produce a hydroperoxyl radical and oxygen. As a result, an increase of the humidity favors the loss of ozone. Hence, the density of ozone decreases with increasing humidity, as also indicated by Fig. 3-4.

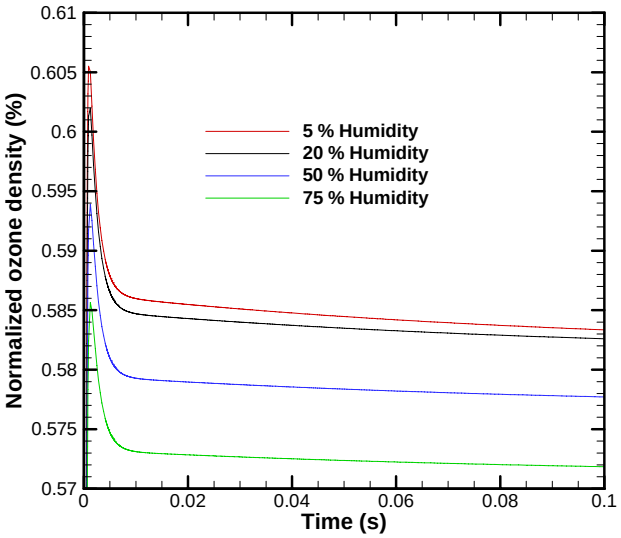

Fig. 4 Calculated ozone density normalized by the background gas density as a function of time for different values of relative humidity at an energy deposition of 0.136 J/cm³.

B. *TCE degradation*

To identify the important destruction reactions for TCE destruction, a pulse was simulated with an energy deposition of 0.136 J/cm³ in a mixture of 1000 ppm TCE. Fig. 5 represents the rates of the different destruction reactions for an energy deposition of 0.136 J/cm³ in a gas mixture of 1000 ppm TCE in humid air (5% relative humidity). The labels correspond to the numbers given for the reactions above. The highest rates in the power pulse can be found for the reactions with atomic oxygen (i.e., reactions 5, 6 and 7, with rates in the order of 10^{16} and 10^{17} cm^{-3} s^{-1}). However, in the afterglow the destruction is dominated by the ClO radicals (i.e., reaction 13) with a maximum rate of 10^{15} cm^{-3} s^{-1}.

Fig. 6 presents the densities of the species which cause destruction of TCE in humid air (5% relative humidity). Similar to the maximum values of the rates we found the highest density for atomic oxygen (10^{16} cm^{-3}) followed by the density of the hydroxyl radical. The densities decrease after pulse termination when the electron density drops to very low values, except for the density of the ClO radical, which drops very slowly even at 0.1 s, explaining why the destruction of TCE is dominated by ClO radicals in the afterglow (see above).

As indicated in Fig. 5, the TCE destruction process is dominated by atomic oxygen. Reactions (5), (6) and (7) have the largest rates and cause most of the destruction. Reaction (5) is found to be one of the production processes of HCl, which is also indicated by Vandenbroucke *et al.* [3] as one of the by-products for TCE destruction. The rates of the destruction with hydroxyl radicals are at least one order of magnitude lower, which can be explained by the lower hydroxyl radical density presented in Fig. 6. However, an increasing humidity will favor the destruction by hydroxyl radicals. The hydroxyl radicals will however also react with ozone (22) and atomic oxygen (24):

$OH + O \rightarrow O_2 + H$ 3.5×10^{-11} cm³/s (24)

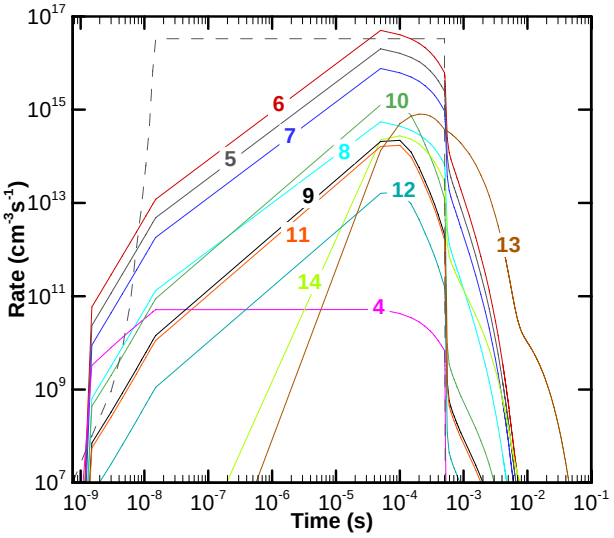

Fig. 5 Calculated rates of the different TCE destruction reactions for an energy deposition of 0.136 J/cm³ in a gas mixture of 1000 ppm TCE in humid air (5% relative humidity). The pulse is indicated by the dashed grey block in the figure

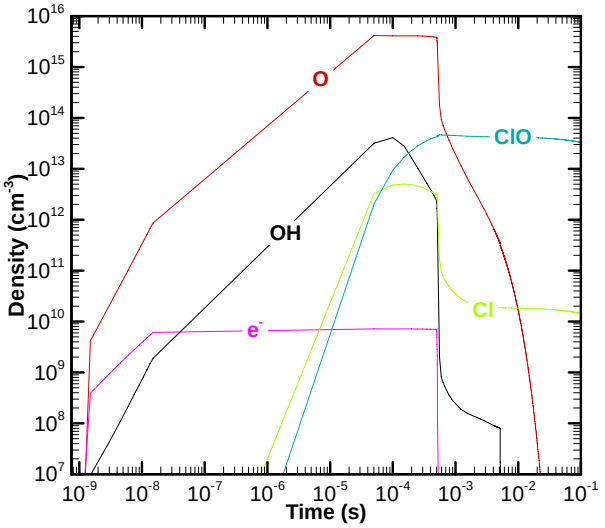

Fig. 6 Calculated species densities as a function of time for an energy deposition of 0.136 J/cm³ in a gas mixture of 1000 ppm TCE in humid air (5% relative humidity).

As indicated above, atomic oxygen is one of the dominant destruction species and an increase in humidity will decrease the density of atomic oxygen. Consequently, the removal efficiency will also decrease. One other important destruction species that must be considered is the ClO radical which has a density of 10^{14} cm^{-3}, even in the afterglow. The rate of the destruction by this species is also sufficient, especially in the afterglow. As a result, it can be concluded that the ClO radical is the dominant destruction species in the afterglow of the plasma. Similar to the loss of atomic oxygen by reaction with hydroxyl radicals, the ClO radical reacts with hydroxyl radicals to form HCl.

$OH + ClO \rightarrow HCl + O_2$ 5×10^{-11} cm³/s (25)

Hence, the removal efficiency also decreases in the afterglow for an increasing humidity.

V. Conclusion

A zero-dimensional plasma-chemical model was used to study the formation of ozone and the abatement of TCE by non thermal plasma. Experiments were carried out to qualitatively validate the model. The following conclusions were derived from this study.

1. The ozone formation increases with the energy deposition and decreases with the relative humidity of the air.
2. The destruction of TCE is mainly dominated by atomic oxygen and to a lesser extent by OH radicals.
3. In the afterglow of the discharge, the destruction is dominated by ClO radicals.
4. When the relative humidity increases, the destruction is favored by OH radicals.

In our future work we will extend the validation of nitrogen metastable species by doing experiments in pure wet and dry nitrogen.

Acknowledgment

We are very grateful to M. Kushner and group members for providing the global_kin code and the useful advice. This work was carried out using the Turing HPC infrastructure at the CalcUA core facility of the Universiteit Antwerpen, a division of the Flemish Supercomputer Center VSC, funded by the Hercules Foundation, the Flemish Government (department EWI) and the Universiteit Antwerpen. We also acknowledge financial support by an IOF-SBO project of the University of Antwerp. R. Morent kindly acknowledges the support of the Research Foundation Flanders (FWO-Belgium) through a postdoctoral research fellowship.

References

[1] A. M. Vandenbroucke, R. Morent, N. De Geyter, C. Leys, "Non-thermal plasmas for non-catalytic and catalytic VOC abatement," J. Hazard. Mater., vol. 195, pp. 30-54, nov. 2011.

[2] D. Evans, L. A. Rosocha, G. K. Anderson, J. J. Coogan, M. J. Kushner, "Plasma remediation of trichloroethylene in silent discharge plasmas," J. Appl. Phys., vol. 74, no. 9, pp. 5378-5386, nov. 1993.

[3] A. M. Vandenbroucke, M. T. Nguyen Dinh, J. M. Giraudon, R. Morent, N. De Geyter, J. F. Lamonier, C. Leys, "Qualitative by-product identification of plasma-assisted TCE abatement by mass spectroscopy and Fourier-transform infrared spectroscopy," Plasma Chem. Plasma Process., vol. 31, no. 5, pp. 707-718, oct. 2011.

[4] R. Dorai, M. J. Kushner, "Consequences of propene and propane on plasma remediation of NO_x," J. Appl. Phys., vol. 88, no. 6, pp. 3739-3747, sep. 2000.

[5] S. Futamura, T. Yamamoto, "Byproduct identification and mechanism determination in plasma chemical decomposition of trichloroethylene," IEEE Trans. Ind. Appl., vol. 33, no. 2, pp. 447-453, mar.-apr. 1997.

[6] N. Blin-Simiand, S. Pasquiers, F. Jorand, C. Postel, J. R. Vacher, “Removal of formaldehyde in nitrogen and in dry air by a DBD: importance of temperature and role of nitrogen metastable states,” J. Phys. D - Appl. Phys., vol. 42, no. 12, 122003, june 2009.

[7] S.B. Han, T. Oda, “Decomposition mechanism of trichloroethylene based on by-product distribution in the hybrid barrier discharge plasma process,” Plasma Sources Sci. Technol., vol. 16, no. 2, pp. 413-421, may 2007

[8] Y. Akishev, O. Goossens, T. Callebaut, C. Leys, A. Napartovich, N. Trushkin, “The influence of electrode geometry and gas flow on corona-to-glow and glow-to-spark threshold currents in air,” J. Phys. D - Appl. Phys., vol. 34, no. 18, pp. 2875-2882, sep. 2001.